

Highly defective graphene: A key prototype of 2D anderson insulators

Aurélien Lherbier(✉), Stephan Roche, Oscar A. Restrepo, Yann-Michel Niquet, Arnaud Delcorte, and Jean-Christophe Charlier

Nano Res., **Just Accepted Manuscript** • DOI: 10.1007/s12274-013-0309-7
<http://www.thenanoresearch.com> on March 19, 2013

© Tsinghua University Press 2013

Just Accepted

This is a “Just Accepted” manuscript, which has been examined by the peer-review process and has been accepted for publication. A “Just Accepted” manuscript is published online shortly after its acceptance, which is prior to technical editing and formatting and author proofing. Tsinghua University Press (TUP) provides “Just Accepted” as an optional and free service which allows authors to make their results available to the research community as soon as possible after acceptance. After a manuscript has been technically edited and formatted, it will be removed from the “Just Accepted” Web site and published as an ASAP article. Please note that technical editing may introduce minor changes to the manuscript text and/or graphics which may affect the content, and all legal disclaimers that apply to the journal pertain. In no event shall TUP be held responsible for errors or consequences arising from the use of any information contained in these “Just Accepted” manuscripts. To cite this manuscript please use its Digital Object Identifier (DOI®), which is identical for all formats of publication.

Highly Defective Graphene: a key prototype of 2D Anderson insulators

Aurélien Lherbier¹ *, Stephan Roche^{2,3}, Oscar A. Restrepo⁴, Yann-Michel Niquet⁵, Arnaud Delcorte⁴, and Jean-Christophe Charlier¹

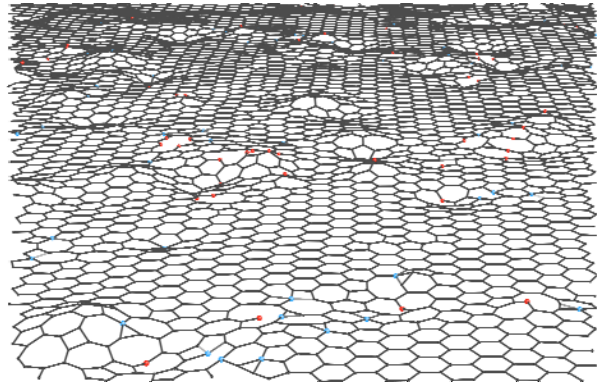
¹ Université catholique de Louvain (UCL), Institute of Condensed Matter and Nanoscience (IMCN), NAPS-ETSF, Chemin des étoiles 8, 1348 Louvain-la-Neuve, Belgium

² CIN2 (ICN-CSIC) and Universitat Autònoma de Barcelona, Catalan Institute of Nanotechnology, Campus UAB, 08193 Bellaterra (Barcelona), Spain

³ ICREA, Institució Catalana de Recerca i Estudis Avançats, 08070 Barcelona, Spain

⁴ Université catholique de Louvain (UCL), Institute of Condensed Matter and Nanoscience (IMCN), BSMA, Place Croix du Sud 1 (Boltzmann), 1348 Louvain-la-Neuve, Belgium

⁵ L_Sim, SP2M, UMR-E CEA/UJF-Grenoble 1, INAC, 17 rue des Martyrs, 38054 Grenoble Cedex 9, France.



Theoretical predictions of electronic structure and transport properties in Highly Defective Graphene (HDG). Simulations reveal mean free paths as low as 1nm and strong Anderson localization phenomena, suggesting HDG as a remarkable prototype of 2D Anderson insulator.

Highly Defective Graphene: a key Prototype of 2D Anderson Insulators.

Aurélien Lherbier¹(✉), Stephan Roche^{2,3}, Oscar A. Restrepo⁴, Yann-Michel Niquet⁵, Arnaud Delcorte⁴, and Jean-Christophe Charlier¹

¹ Université catholique de Louvain (UCL), Institute of Condensed Matter and Nanoscience (IMCN), NAPS-ETSF, Chemin des étoiles 8, 1348 Louvain-la-Neuve, Belgium

² CIN2 (ICN-CSIC) and Universitat Autònoma de Barcelona, Catalan Institute of Nanotechnology, Campus UAB, 08193 Bellaterra (Barcelona), Spain

³ ICREA, Institució Catalana de Recerca i Estudis Avançats, 08070 Barcelona, Spain

⁴ Université catholique de Louvain (UCL), Institute of Condensed Matter and Nanoscience (IMCN), BSMA, Place Croix du Sud 1 (Boltzmann), 1348 Louvain-la-Neuve, Belgium

⁵ L_Sim, SP2M, UMR-E CEA/UJF-Grenoble 1, INAC, 17 rue des Martyrs, 38054 Grenoble Cedex 9, France.

Received: day month year / Revised: day month year / Accepted: day month year (automatically inserted by the publisher)

© Tsinghua University Press and Springer-Verlag Berlin Heidelberg 2011

ABSTRACT

Electronic structure and transport properties of highly defective two-dimensional sp^2 graphene are investigated theoretically. Classical molecular dynamics are used to generate large graphene planes containing a considerable amount of defects. Then, a tight-binding Hamiltonian validated by ab initio calculations is constructed in order to compute quantum transport within a real-space order-N Kubo-Greenwood approach. In contrast to pristine graphene, the highly defective sp^2 carbon sheets exhibit high density of states at charge neutrality point raising challenging questions concerning the electronic transport of associated charge carriers. The analysis of the electronic wavepacket dynamics actually reveals extremely strong multiple scattering effects yielding to mean free paths as low as 1nm and localization phenomena. Consequently, highly defective graphene is envisioned as a remarkable prototype of 2D Anderson insulating materials.

KEYWORDS

Graphene, electronic transport, Anderson insulators, localization

1. Introduction

Graphene's outstanding electronic and mechanical properties [1-3] are currently used to engineer novel types of flexible and transparent electrodes [4, 5]. However, the presently CVD [6] grown large-scale graphene samples remain rich in defects and grain boundaries which can limit the performances of related devices [7]. The detrimental effects of such structural imperfections on charge mobility are difficult to circumvent and require close inspection. Theoretically, the impact of extended lines of defects and of single structural defects (as produced by rapid thin-film growth or using ion-irradiation) has been now widely studied [8-13], revealing interesting features such as electron-hole transport asymmetry [14] due to the presence of defect-induced resonances.

Recently, using controlled electron irradiation, Kotakoski *et al.* [15] have reported on the possible engineering of a new two-dimensional amorphous carbon lattice. The latter is composed of sp^2 -hybridized carbon atoms, arranged as a random tiling of the plane with polygons including four-membered rings. So far, only few studies, mostly theoretical [16-19], have examined this new allotrope of the sp^2 carbon family. A large increase of the density of states at the charge neutrality point is an unvarying prediction concerning these amorphous carbon lattices. However, their transport properties are still debated. Based on a stochastic quenching method, these two-dimensional amorphous carbon lattices have been suggested to entail a metallic behavior, suitable for transparent electrodes applications [18], while other approaches have reported on the presence of localized states [16] which should greatly deteriorate the transport properties leading eventually to an insulating behavior. Therefore, this new carbon allotrope system deserves more detailed analysis to unravel accurately its electronic and transport properties.

In this article, a realistic model of this two-dimensional amorphous carbon system is investigated, namely a highly defective graphene structure. In contrast to fully amorphous graphene membranes, highly defective graphene systems are composed of patches of highly defective regions together with reconstructed pristine area. Here, such highly defective graphene structures are created using classical molecular dynamics simulations. Although the obtained defective graphene models also exhibit high density of states close to the charge neutrality point (Dirac point for pristine graphene), the resulting transport properties display features typical of a strong Anderson insulator, with elastic mean free paths below 1 nanometer, low mobilities in the order of $10 - 100 \text{ cm}^2\text{V}^{-1}\text{s}^{-1}$ and considerable effect of quantum interferences. Despite our calculations predict that two-dimensional highly defective carbon lattices are not the best suited graphene-based system for applications as conductive materials in electronic devices, the present study suggests that such highly defective graphene-based prototype should offer intriguing possibilities to explore theoretically and experimentally the physics of two-dimensional Anderson insulators.

2. Results and Discussion

2.1. Highly defective graphene structure from classical molecular dynamics

The highly defective graphene (HDG) structures are generated by classical molecular dynamics (CMD) simulations. Starting from a pristine graphene square sheet ($200 \times 200 \text{ nm}^2$, i.e. $\sim 1.5 \times 10^6$ carbon atoms), a small random in-plane displacement $\delta\mathbf{R}$ is applied to each atomic position with $|\delta\mathbf{R}| \leq d_{cc}/3$, $d_{cc} = 1.42 \text{ \AA}$ being the carbon-carbon interatomic distance. This *randomized graphene sheet* serves as an input for the CMD calculation (Fig. 1(a)). The evolution of atomic positions are driven by an interatomic Tersoff-type potential (REBO) developed by Brenner *et al.* [20, 21].

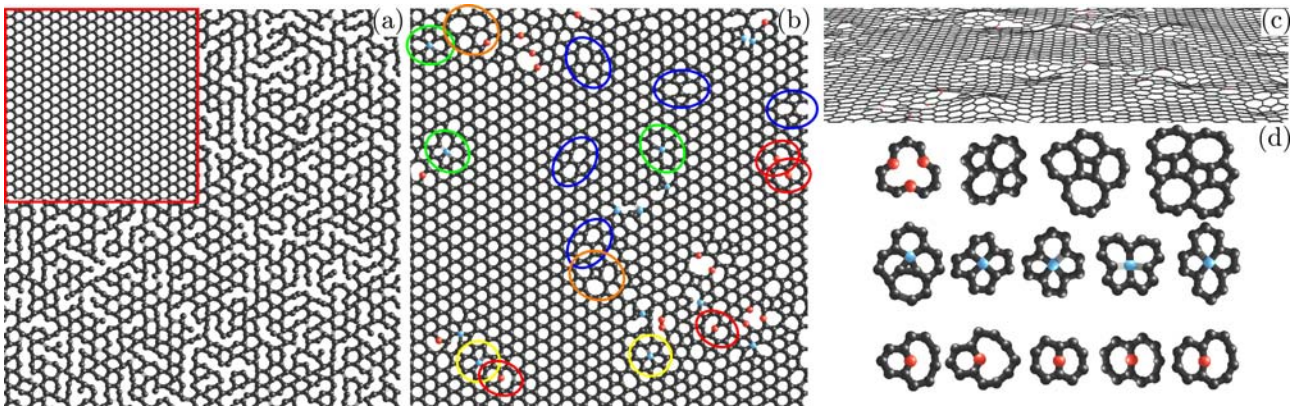


Figure 1 Geometry of highly defective graphene. (a) Randomized graphene layer (inset: starting pristine graphene layer) used as input for the CMD simulation. (b) Structure model of highly defective graphene following CMD at $T_L = 1200$ K. Specific defects of the same type are indicated with circles of the same color. (c) Structure model after the second CMD simulation allowing out-of-plane deformations. The square piece of graphene presented in (a), (b) and (c) is only a small part of the whole system which is $200 \times 200 \text{ nm}^2$. (d) Non-exhaustive list of the most frequently observed structural defects isolated from the plane. 2-, 3-, and 4-coordinated carbon atoms are depicted using red, black, and blue spheres, respectively.

In the CMD simulations, periodic boundary conditions are applied and, to promote the healing of highly unstable defects, a large window of thermostatic Langevin temperatures (T_L) from 0 K to 2600 K is probed. The total number of carbon atoms being kept constant, the CMD simulations are hence performed in the context of the *canonical ensemble*. Moreover, in a first step, velocities along the perpendicular direction to the sheet are set to zero, thus confining the atoms in the plane. After 500 fs, the atomic positions do not change anymore significantly. The dynamics is however continued till 2000 fs to allow the occurrence of low probability events. Then, a snapshot of the system is taken. A structural disorder model is obtained typically containing domains of strongly defective graphene together with preserved regions maintaining the local honeycomb lattice although slightly deformed (Fig. 1(b)). In a second step, another CMD simulation, with T_L fixed to 10 K, is conducted allowing out-of-plane deformations (Fig. 1(c)). A similar procedure has been applied in reference [18]. This last step can eventually yields to the ejection out-of-plane of few atoms.

A huge variety of structural defects including some exotic ones can be observed in the defective graphene plane (as partially illustrated in Fig. 1(d)). These structural modifications consist in non-hexagonal rings, incorporating 2-, 3-, and/or 4-coordinated carbon atoms. Occasionally, dangling carbon atoms (1-coordinated) are generated but in extremely small quantity (discarded in subsequent transport calculations since they are particularly unstable), while 5-coordinated carbon atoms have never been observed. 2-coordinated carbon atoms are observed in conjunction with dangling bonds or short linear atomic chains. At last, 4-coordinated carbon atoms are mostly detected at the intersection of various membered rings. However, the number of low- and high-coordinated carbon atoms is found to decrease with Langevin temperature as depicted in Fig. 2(a). For instance, at $T_L = 2600$ K, 2- and 4-coordinated carbon atoms represent less than 2% in the whole sheet. After the second CMD simulation, a tiny amount of carbon atoms ($< 0.0033\%$) are ejected from the plane, thus creating small holes in the sheet around which short atomic chains are occasionally observed. Consequently, after this second CMD simulation, slightly more 1-coordinated carbon

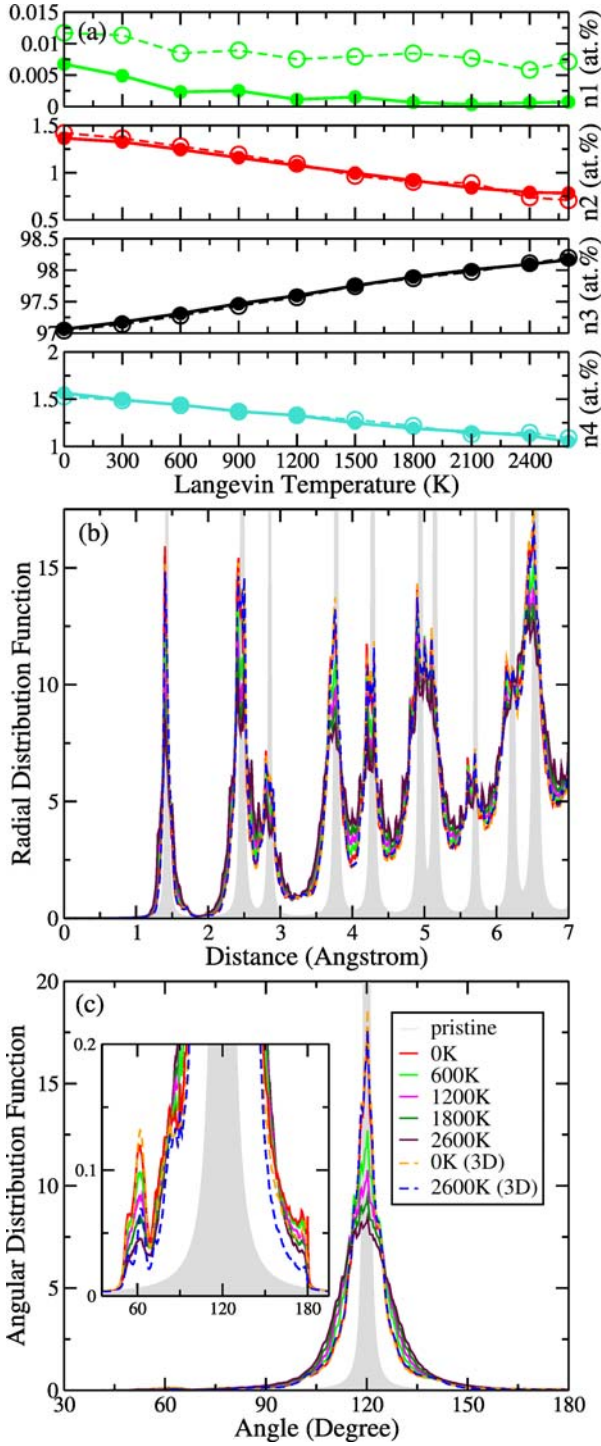


Figure 2 (a) Percentage of carbon atoms exhibiting coordination numbers from 1 ($n1$) to 4 ($n4$) as a function of T_L . Radial (b) and angular (c) distribution functions of pristine (gray filled curves) and HDG as a function of T_L . Results after the 3D CMD are plotted in dashed lines.

atoms are counted as shown in Fig. 2(a) (dashed

lines), although the general coordination number statistic is almost unchanged compared to the 2D approximation. Amongst the large variety of defects, some well-known defects are more frequently observed such as Stone-Wales defects, vacancies, but also various forms of *double ring* defects composed of 6 or higher membered carbon rings (such as the 6-9,6-10,7-7,7-8, and 7-9 defects displayed in the last row in Fig. 1(d)). Different topologies of planar 4-coordinated carbon with a 90° angle configuration (5555, 555-6, 55-66) are also detected for not too high T_L . Interestingly, these metastable geometries have been predicted by R. Hoffmann *et al.* in 1970 [22] and have also been proposed to play a key role in the migration of vacancies in irradiated carbon nanotubes [23] and graphene [24]. The planar HDG structures obtained using the Brenner potential within CMD simulations can eventually lead to small internal stress inducing metastable carbon geometries such as the 4-coordinated carbon atoms. However, these metastable geometries tend to disappear by self-healing with increasing T_L . In addition, their small amount should not alter the following electronic transport results. The presence of a large number of pentagons and heptagons is expected to induce some puckering of the HDG layer [17]. However, using an accurate first principle-based stochastic quenching method, a recent study has predicted that the buckling amplitude shall be small in amorphous graphene planes (1.7 Å) due to “an averaging of defect-induced buckling forces” [18]. Indeed, out-of-plane deformations induced locally by pentagons and heptagons tend to annihilate themselves, as it occurs for instance in a 555-777 divacancy defect whose stable geometry is planar [9, 14]. The much larger system obtained here is slightly different from Refs. [16-18], since it is not completely amorphous and contains randomly distributed ordered areas [25]. In the present case, the maximum deviation from the plane is estimated to be ~ 2.5 Å. The buckling is mostly observed in regions containing non

3-coordinated carbon atoms, while reconstructed honeycomb lattice area appear almost at (Fig. 2(c)). Nevertheless, any corrugation of the HDG would eventually be reduced by a flat underneath substrate such as hexagonal boron nitride [26, 27].

The HDG sheets can be further characterized by analyzing the radial and angular distribution functions (RDF/ADF). In principle, the RDF of pristine graphene presents Dirac peaks at the 1st, 2nd, 3rd... nearest neighbors (-nn) distances. However, these peaks have been broadened by a Lorentzian function in Fig. 2(b) to enhance the readability of the plots. The same broadening has been used for the RDF of the HDG. However, an additional broadening can be observed, which is rather small for the 1st-nn peak, but increases with distance (i.e. for next-nn). This is a clear signature of a relative amorphization of the system. The broadening is also found to increase with T_L [28] in 2D CMD simulations, while for subsequent 3D CMD simulations (dashed lines in Fig. 2(b-c)), the RDF curves are all similar to the 2D CMD results obtained for $T_L = 0$ K. The ADF of the pristine graphene depicted in Fig. 2(c), is composed of a single peak at 120° , while in the HDG layer, small other peaks emerge at 60° and 180° due to the incorporation of defects (see inset). A tiny peak at 90° , resulting from the few 4-coordinated carbon atoms, is also observed at low T_L but disappears for higher T_L . In addition, the main peak around 120° is clearly broadened. Again, this broadening is larger for higher T_L , which tends to demonstrate a more pronounced disordered character for higher T_L . However, as observed for the RDF, when performing the final 3D CMD the ADF curves go back to the result of 2D CMD at $T_L = 0$ K. In the following, the electronic and transport properties of HDG planes will be investigated using a *tight-binding* framework together with an efficient real-space Kubo-Greenwood formalism. The presence of a large variety of defects together with buckling renders the *tight-binding* parameterization very tedious. Therefore, since RDF and ADF of

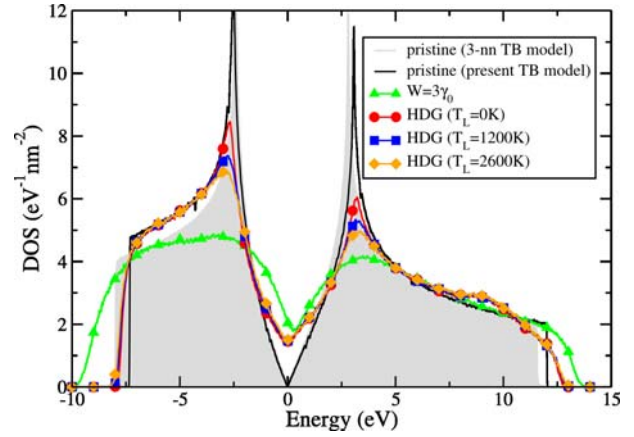


Figure 3 Density of states of pristine graphene, of disordered graphene ($W = 3\gamma_0$), and of three HDG layers obtained using different T_L .

strictly 2D HDG and buckled HDG exhibit about the same coordination statistics, the electronic and transport properties will be computed in 2D HDG structures for the sake of simplicity.

2.2. Electronic Properties

An empirical π - π^* orthogonal *tight-binding* (TB) model [29] was used to explore the electronic properties of HDG. The essential ingredients of the model are a hopping term $\gamma(d) = \gamma_0 \exp(-3.37 (d/d_{cc} - 1))$, with $\gamma_0 = -3.0933$ eV, for p_z orbitals distant up to $d = 5$ Å one from each other, while the onsite energy is set to $\epsilon_{pz} = 0.79745$ eV so that Dirac point lies at 0 eV. A negative sign is added to $\gamma(d)$ for 2nd-nn, as an effect of orthogonality constraints. Figure 3 displays the density of states (DOS) obtained for pristine graphene using the present TB model, which is in good agreement with a 3rd-nn π - π^* orthogonal TB model validated by *ab initio* calculations [14]. The DOS of HDG obtained at different T_L are also presented. A transition from a zero-gap semiconductor to a metallic-like phase is observed. Indeed, in HDG, a large increase of DOS is observed near the charge neutrality point. This increase of DOS can actually be explained by an overlap of numerous resonances induced by the presence of a huge number of structural defects of various natures

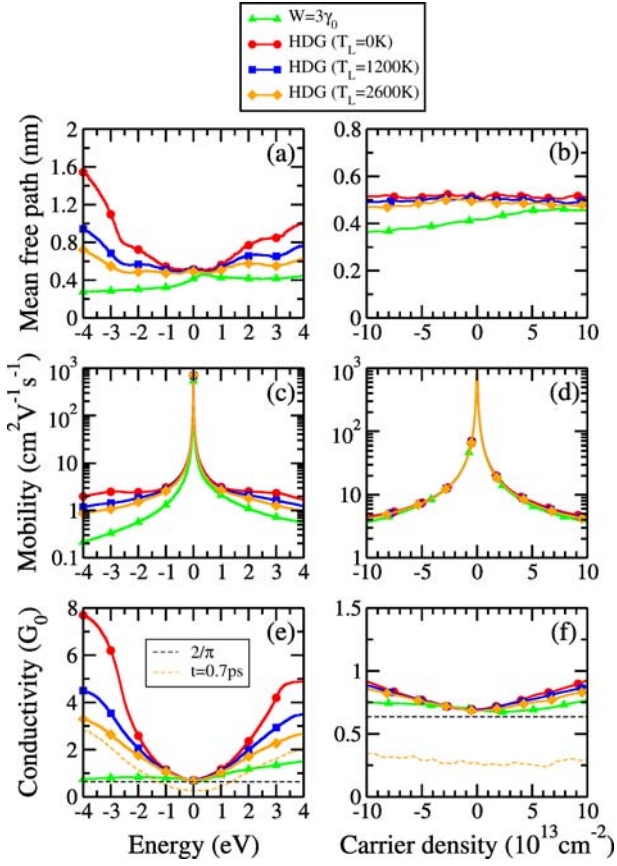


Figure 4 Transport properties of disordered graphene ($W = 3\gamma_0$) and of HDG obtained for three different T_L . (a-b) Electron/Hole mean free paths. (c-d) Electron/Hole mobilities. (e-f) Electron/Hole conductivities. (a), (c), and (e) are given as a function of energy while (b), (d), (f) are given as a function of carrier density (negative densities corresponding to holes).

[30]. Meanwhile, a smoothening of the two van Hove singularities is noticed on the DOS of HDG. These two features are typical of a strong Anderson disorder [31]. The latter is a well-known academic disorder model which consists in applying random fluctuations of the onsite energies: $\delta\varepsilon_{pz} = [-W/2, W/2]$. For comparison, the DOS of a graphene plane subjected to Anderson disorder using $W = 3\gamma_0$ (strong disorder) is also presented in Fig. 3 (green line with triangles). In that case, the van Hove singularities as well as the outer part of the spectrum are even more smoothed out because the Anderson disorder for $W = 3\gamma_0$ impacts the entire spectrum while for HDG planes, the various structural defects

produce mainly energy resonances close to the Dirac point.

2.3. Electronic Transport

The transport properties of the HDG layers are computed from the dynamics of electronic wavepackets with an order- N Kubo-Greenwood method [14, 31-36]. In such technique, the key quantity is time evolution of the diffusion coefficient ($D(E,t)$) from which the transport properties are explored. At very short times, the wavepacket dynamics is quasi-ballistic and $D(E,t)$ is linear in time. Then it becomes diffusive as the carriers get scattered by the disorder, and $D(E,t)$ reaches a maximum value from which we extract the mean free path ($l_e(E)$), the semiclassical conductivity ($\sigma_{sc}(E)$) and the mobility ($\mu(E)$) (see Methods section). At even longer times, localization due to multiple scattering events per carrier causes $D(E,t)$ to decrease.

In HDG, the computed mean free path is found to be weakly dependent on the energy (Fig. 4(a)), being almost constant ($l_e \sim 0.5 - 1.5 \text{ nm} \sim 4-10 \text{ dcc}$) over a large window ($[-4,+4] \text{ eV}$). In Fig. 4(c), the charge carrier mobility derived from $\mu(E) = \sigma_{sc}(E)/(e n(E))$ ($n(E)$ being the carrier density) is found to be of the order of $10-100 \text{ cm}^2\text{V}^{-1}\text{s}^{-1}$ which is 2-3 orders of magnitudes smaller than the experimental measurements on usual graphene samples [26, 37]. Figure 4(e) presents the semiclassical conductivity of the HDG sheet as a function of charge carrier energy. At the Dirac point, σ_{sc} exhibits a minimal value slightly above the universal minimum conductivity $\sigma_{sc}^{\min} = 4e^2/\pi h$ predicted for short range disorder potential, and whose origin is now well established [38-42]. Our results demonstrate that such a value could also be measured in a HDG at room temperature [43]. The mean free paths, the mobilities, and the conductivities in HDG are also plotted as a function of the charge carrier density in Fig. 4(b), Fig. 4(d) and Fig. 4(f) respectively. Close to the Dirac point, $l_e(E)$, $\mu(E)$ and $\sigma_{sc}(E)$ obtained for a strong Anderson disorder ($W = 3\gamma_0$) are found very similar

to the ones observed in the present HDG layers (see green lines with triangle symbols in Fig. 4).

2.4. Localization Effects

Due to the predicted short mean free paths, strong contributions of quantum interferences are expected at low temperatures. Compelling evidences of such interferences are exhibited by the time-dependence of the ratio $D(t)/D_{\max}$. Figure 5 illustrates this ratio at three different energies (close to/far from the Dirac point). $D(t)/D_{\max}$ quickly decays because of strong localization effects, suggesting a very short localization length ξ . Using the scaling theory of localization [44], ξ can be actually estimated from $\xi(E) = \sqrt{2} l_e(E) \exp(\pi \hbar \sigma_{sc}(E)/2e^2)$. From our calculations, $\xi \sim 5\text{nm}$ is estimated for $E = 0\text{ eV}$ (where $\sigma_{sc} = \sigma_{sc}^{\min}$), which appears to be extremely short. Moreover, for E in $[-1,+1]\text{ eV}$, ξ is predicted to be smaller than 20nm which is much shorter than for weakly disordered (e.g. doped) graphene [45]. The build-up of quantum interferences beyond the short-time/short-lengths diffusive regime localizes the carriers and decreases the actual (quantum) conductivity of the system in large HDG samples (or equivalently at long times in our calculations). As an illustration, the quantum conductivity computed for a HDG layer ($T_L = 2600\text{ K}$) from the diffusivity at a longer time $t = 0.7\text{ ps}$ [46] is plotted with a dashed-dotted line in Fig. 4(e-f). It is already significantly lower than σ_{sc} computed from D_{\max} obtained at shorter times. At low temperatures, the electron-phonon scattering cannot efficiently break phase coherence, so the conductivity of HDG layers is expected to decrease exponentially with size (and eventually vanish) beyond a few ξ , i.e. at most a few tens of nanometers. Localization should also lead to an easily observable variable range hopping behavior in the temperature dependence of the conductivity. Similar strong localization effects are obtained in the case of an Anderson disorder model. Eventually, the small puckering, as obtained in the 3D CMD simulations, would introduce slight additional sp^3 hybridization of carbon atoms, which

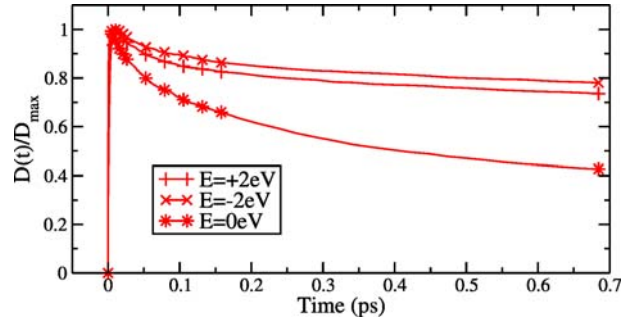


Figure 5 Normalized diffusion coefficient $D(t)/D_{\max}$ in HDG obtained at $T_L=0\text{ K}$ and for three different energies $E=+2, -2,$ and 0 eV (plus, crosses, and stars signs).

is expected to increase the overall disorder strength and reinforce the present conclusion concerning the Anderson insulating behavior of HDG.

3. Conclusions

Large-sized highly defective graphene sheets generated by molecular dynamics exhibit enhanced density of states close to the charge neutrality point, together with very short mean free paths (below 1 nm), low mobilities and strong localization effects. These highly defective graphene sheets are therefore suggested to become a genuine playground for fundamental exploration of Anderson localization phenomena in two-dimensional systems. Raman analysis [47, 48] and low temperature transport measurements [49, 50] in such sp^2 Anderson insulating amorphous graphene layers would be desirable to confirm those predictions.

4. Methods

A real-space order- N Kubo-Greenwood approach is employed to compute the different transport properties. The latter are inferred from the dynamics of the wavepackets propagation. This dynamics is monitored through the time-dependent diffusion coefficient $D(E,t) = \Delta R^2(E,t)/t$, with E the energy of the carriers, $\Delta R^2 = \Delta X^2 + \Delta Y^2$, and $\Delta X^2(E,t) = \text{Tr}[\delta(E-H)|X(t)-X(0)|^2]/\text{Tr}[\delta(E-H)]$ the quadratic spreading along the x direction. Tr is the trace over p_z orbitals and $\text{Tr}[\delta(E-H)]/S = \rho(E)$ is the total DOS (per

unit of area S). The time dependent Schrödinger equation is solved up to $t = 700$ fs thanks to an efficient expansion of the time evolution operator in a basis of Chebyshev polynomials ($U(t) = \prod_{n=0}^{N-1} \exp(i H \Delta t / \hbar)$ with Δt the time step). The time evolution operator $U(t)$ is used to compute both position operators $X(t)$ and $Y(t)$, expressed in the Heisenberg representation ($X(t) = U^\dagger(t)X(0)U(t)$). Transport calculations are averaged over many runs with different initial random phase wavepackets. At very short times, the wavepacket dynamics is quasi-ballistic, so that $D(E,t) \sim v^2(E)t$, where $v(E)$ is the carrier velocity. Then it becomes diffusive as the carriers get scattered by the disorder, and $D(E,t)$ reaches a maximum value $D_{\max}(E) = 2v(E)l_e(E)$, where $l_e(E)$ is the mean free path. The semiclassical conductivity then reads $\sigma_{sc}(E) = \frac{1}{4} e^2 \rho(E)D_{\max}(E)$. At even longer times, localization due to multiple scattering events per carrier causes $D(E,t)$ to decrease.

In the present study, the Anderson disorder model (white noise potential) commonly used in the TB framework is likened to HDG layers. Random fluctuations ($\delta\varepsilon_{pz}$) are imposed on all onsite energies thus affecting the diagonal of the TB Hamiltonian. In such a model, the disorder strength is given by a single parameter W , which can be tuned from very small to high energies, or equivalently from weak to strong disorder. The onsite fluctuations terms are random but constrained within a range of $[-W/2, W/2]$. Usually, when the disorder strength W exceeds the width of the electronic spectrum of the material, the disorder is considered as very strong since it can alter the whole spectrum. In the present case, $W = 3\gamma_0 \sim 9\text{eV}$ is a quite strong disorder for graphene (π - π^* model). For more details, the reader is referred to a previous study [31].

Acknowledgements

J.-C.C., A.D., and A.L. acknowledge financial support from the Belgium FNRS. S.R. acknowledges the Spanish Ministry for financial support through the project MAT2012-33911. This work is connected to the ARC Graphene Nano-electromechanics (N.° 11/16-037), the ETSF e-I3 project (N.° 211956), and the NANOSIM-GRAPHENE (ANR-09-NANO-016-01). Computational resources are provided by the UCL-CISM. Free access to the SPUT code was granted by Prof. B.J. Garrison.

References

- [1] Kim, K. S.; Zhao, Y.; Jang, H.; Lee, S. Y.; Kim, J. M.; Kim, K. S.; Ahn, J.-H.; Kim, P.; Choi, J.-Y.; Hong, B. H. Large-scale pattern growth of graphene films for stretchable transparent electrodes. *Nature* **2009**, *457* (7230), 706–710.
- [2] Novoselov, K.S. Nobel Lecture: Graphene: Materials in the Flatland. *Rev. Mod. Phys.* **2011**, *83* (3), 837–849.
- [3] de Heer, W. A.; Berger, C.; Wu, X.; First, P. N.; Conrad, E. H.; Li, X.; Li, T.; Sprinkle, M.; Hass J.; Sadowski, M. L.; Potemski, M.; Martinez, G. Epitaxial graphene. *Solid State Commun.* **2007**, *143* (1-2), 92–100.
- [4] Wang, X.; Zhi, L.; Müllen, K. Transparent, Conductive Graphene Electrodes for Dye-Sensitized Solar Cells. *Nano Lett.* **2008**, *8* (1), 323–327.
- [5] Bae, S.; Kim, H.; Lee, Y.; Xu, X.; Park, J.-S.; Zheng, Y.; Balakrishnan, J.; Lei, T.; Kim, H. R.; Song, Y. I.; Kim, Y.-J.; Kim, K. S.; Özyilmaz, B.; Ahn, J.-H.; Hong, B. H.; Iijima, S. Roll-to-roll production of 30-inch graphene films for transparent electrodes. *Nature Nanotech.* **2010**, *5* (8), 574–578.
- [6] CVD stands for Chemical Vapor Deposition.
- [7] Ferreira, A.; Xu, X.; Tan, C.-L.; Bae, S.-K.; Peres, N. M. R.; Hong, B.-H.; Özyilmaz, B.; Castro Neto, A. H. Transport properties of graphene with one-dimensional charge defects. *Eur. Phys. Lett.* **2011**, *94* (2), 28003–28008.
- [8] Krasheninnikov, A. V.; Banhart, F. Engineering of nanostructured carbon materials with electron or ion beams. *Nature Materials* **2007**, *6* (10), 723–733.
- [9] Banhart, F.; Kotakoski, J.; Krasheninnikov, A. V. Structural Defects in Graphene. *ACS Nano* **2011**, *5* (1), 26–41.
- [10] Cockayne, E.; Rutter, G. M.; Guisinger, N. P.; Crain, J. N.; First, P. N.; Stroscio, J. A. Grain boundary loops in graphene. *Phys. Rev. B* **2011**, *83* (19), 195425–195431.
- [11] Botello-Méndez, A. R.; Declerck, X.; Terrones, M.; Terrones, H.; Charlier, J.-C. Onedimensional extended lines of divacancy defects in graphene. *Nanoscale* **2011**, *3* (7), 2868–2872.
- [12] Lusk, M. T.; Wu, D. T.; Carr, L. D. Graphene

- nanoengineering and the inverse Stone-Thrower-Wales defect. *Phys. Rev. B* **2010**, *81* (15), 155444–155452.
- [13] Yazyev, O. V.; Louie, S. G. Electronic transport in polycrystalline graphene. *Nature Materials* **2010**, *9* (10), 806–809.
- [14] Lherbier, A.; Dubois, S. M.-M.; Declerck, X.; Roche, S.; Niquet, Y. M.; Charlier, J.-C. Two-Dimensional Graphene with Structural Defects: Elastic Mean Free Path, Minimum Conductivity, and Anderson Transition. *Phys. Rev. Lett.* **2011**, *106* (4), 046803–046806.
- [15] Kotakoski, J.; Krashenninnikov, A. V.; Kaiser, U.; Meyer, J. C. From Point Defects in Graphene to Two-Dimensional Amorphous Carbon. *Phys. Rev. Lett.* **2011**, *106* (10), 105505–105508.
- [16] Kapko, V.; Drabold, D. A.; Thorpe, M. F. Electronic structure of a realistic model of amorphous graphene. *Phys. Status Solidi B* **2010**, *247* (5), 1197–1200.
- [17] Li, Y.; Inam, F.; Kumar, A.; Thorpe, M. F.; Drabold, D. A. Pentagonal puckering in a sheet of amorphous graphene. *Phys. Status Solidi B* **2011**, *248* (9), 2082–2086.
- [18] Holmström, E.; Fransson, J.; Eriksson, O.; Lizárraga, R.; Sanyal, B.; Bhandary, S.; Katsnelson, M. I. Disorder-induced metallicity in amorphous graphene. *Phys. Rev. B* **2011**, *84* (20), 205414–205418.
- [19] Tuan D. V.; Kumar A.; Roche S.; Ortmann F.; Thorpe M. F.; Ordejon P. Insulating behavior of an amorphous graphene membrane. *Phys. Rev. B (R)* **2012**, *86* (12), 121408–121412.
- [20] Brenner, D. W.; Shenderova, O. A.; Harrison, J. A.; Stuart, S. J.; Ni, B.; Sinnott, S. B. A second-generation reactive empirical bond order (REBO) potential energy expression for hydrocarbons. *J. Phys. Cond. Matt.* **2002**, *14* (4), 783–802.
- [21] Stuart, S. J.; Tutein, A. B.; Harrison, J. A. A reactive potential for hydrocarbons with intermolecular interactions. *J. Chem. Phys.* **2000**, *112* (14), 6472–6486.
- [22] Hoffmann, R.; Alder, R. W.; Wilcox, C. F. Planar tetracoordinate carbon. *J. Am. Chem. Soc.* **1970**, *92* (16), 4992–4993.
- [23] Ajayan, P. M.; Ravikumar, V.; Charlier, J.-C. Surface Reconstructions and Dimensional Changes in Single-Walled Carbon Nanotubes. *Phys. Rev. Lett.* **1998**, *81* (7), 1437–1440.
- [24] Wang, B.; Puzyrev, Y.; Pantelides, S. T. Strain enhanced defect reactivity at grain boundaries in polycrystalline graphene. *Carbon* **2011**, *49* (12), 3983–3988.
- [25] To avoid misleading comparisons between highly defective graphene and amorphous graphene, the first terminology has been preferred and used along the manuscript.
- [26] Dean, C. R.; Young, A. F.; Meric, I.; Lee, C.; Wang, L.; Sorgenfrei, S.; Watanabe, K.; Taniguchi, T.; Kim, P.; Shepard, K. L.; Hone, J. Boron nitride substrates for high-quality graphene electronics. *Nature Nanotech.* **2010**, *5* (10), 722–726.
- [27] Xue, J.; Sanchez-Yamagishi, J.; Bulmash, D.; Jacquod, P.; Deshpande, A.; Watanabe, K.; Taniguchi, T.; Jarillo-Herrero, P.; LeRoy, B. J. Scanning tunnelling microscopy and spectroscopy of ultra-flat graphene on hexagonal boron nitride. *Nature Materials* **2011**, *10* (4), 282–285.
- [28] For a fixed TL , RDF/ADF and transport calculations are performed using only one HDG layer. However, an intrinsic average of the disorder exists due to the large system size.
- [29] Pereira, V. M.; Castro Neto, A. H.; Peres, N. M. R. Tight-binding approach to uniaxial strain in graphene. *Phys. Rev. B* **2009**, *80* (4), 045401–045408.
- [30] Lherbier, A.; Dubois, S. M.-M.; Declerck, X.; Niquet, Y. M.; Roche, S.; Charlier, J.-C. Transport properties of graphene containing structural defects. *Phys. Rev. B* **2012**, *86* (7), 075402–075419.
- [31] Lherbier, A.; Biel, B.; Niquet, Y. M.; Roche, S. Transport Length Scales in Disordered Graphene-Based Materials: Strong Localization Regimes and Dimensionality Effects. *Phys. Rev. Lett.* **2008**, *100* (3), 036803–036806.
- [32] Roche, S.; Mayou, D. Conductivity of Quasiperiodic Systems: A Numerical Study. *Phys. Rev. Lett.* **1997**, *79* (13), 2518–2521.
- [33] Roche, S. Quantum transport by means of $O(N)$ real-space methods. *Phys. Rev. B* **1999**, *59* (3), 2284–2291.
- [34] Ishii, H.; Triozon, F.; Kobayashi, N.; Hirose, K.; Roche, S. Charge transport in carbon nanotubes based materials: a Kubo-Greenwood computational approach. *C.R. Physique* **2009**, *10* (4), 283–296.
- [35] Leconte, N.; Moser, J.; Ordejón, P.; Tao, H.; Lherbier, A.; Bachtold, A.; Alsina, F.; Sotomayor Torres, C. M.; Charlier, J.-C.; Roche, S. Damaging graphene with ozone treatment: a chemically tunable metal-insulator transition. *ACS Nano* **2010**, *4* (7), 4033–4038.
- [36] Radchenko, T. M.; Shylau, A. A.; Zozoulenko, I. V. Influence of correlated impurities on conductivity of graphene sheets: Time-dependent real-space Kubo approach. *Phys. Rev. B* **2012**, *86* (3), 035418–035430.
- [37] Tan, Y.-W.; Zhang, Y.; Bolotin, K.; Zhao, Y.; Adam, S.; Hwang, E. H.; Das Sarma, S.; Stormer, H. L.; Kim, P. Measurement of Scattering Rate and Minimum Conductivity in Graphene. *Phys. Rev. Lett.* **2007**, *99* (24), 246803–246806.
- [38] Shon, N. H.; Ando, T. Quantum Transport in Two-Dimensional Graphite System. *J. Phys. Soc. Jpn.* **1998**, *67* (7), 2421–2429.
- [39] Peres, N. M. R.; Guinea, F.; Castro Neto, A. H. Electronic properties of disordered two-dimensional carbon. *Phys. Rev. B* **2006**, *73* (12), 125411–125433.
- [40] Ostrovsky, P. M.; Gornyi, I. V.; Mirlin, A. D. Electron transport in disordered graphene. *Phys. Rev. B* **2006**, *74* (23), 235443–235462.
- [41] Nomura, K.; MacDonald, A. H. Quantum Transport of Massless Dirac Fermions. *Phys. Rev. Lett.* **2007**, *98* (7), 076602–076605.
- [42] Geim, A. K.; Novoselov, K. S. The rise of graphene. *Nature Materials* **2007**, *6* (3), 183–191.
- [43] The mobility and the conductivity have been computed using a Fermi-Dirac temperature of $T_F = 300\text{K}$ which basically smooths out the quantities obtained at 0K .
- [44] Lee, P. A.; Ramakrishnan, T. V. Disordered electronic systems. *Rev. Mod. Phys.* **1985**, *57* (2), 287–337.

- [45] Lherbier, A.; Blase, X.; Niquet, Y. M.; Triozon, F.; Roche, S. Charge Transport in Chemically Doped 2D Graphene. *Phys. Rev. Lett.* **2008**, *101* (3), 036808–036811.
- [46] The time-dependent quantum conductivity $\sigma(E,t)$ is computed from $\sigma(E,t) = 1/4 e^2 \rho(E) D(E,t)$.
- [47] Ferrari, A. C.; Meyer, J. C.; Scardaci, V.; Casiraghi, C.; Lazzeri, M.; Mauri, F.; Piscanec, S.; Jiang, D.; Novoselov, K. S.; Roth, S.; Geim, A. K. Raman Spectrum of Graphene and Graphene Layers. *Phys. Rev. Lett.* **2006**, *97* (18), 187401–187404.
- [48] Casiraghi, C.; Hartschuh, A.; Qian, H.; Piscanec, S.; Georgi, C.; Fasoli, A.; Novoselov, K. S.; Basko, D. M.; Ferrari, A. C. Raman Spectroscopy of Graphene Edges. *Nano Lett.* **2009**, *9* (4), 1433–1441.
- [49] Liu, G.; Teweldebrhan, D.; Balandin, A. A.; Tuning of Graphene Properties via Controlled Exposure to Electron Beams. *IEEE Trans. on Nanotech.* **2011**, *10* (4), 865–870.
- [50] Teweldebrhan, D.; Balandin, A. A. Modification of graphene properties due to electronbeam irradiation. *Appl. Phys. Lett.* **2009**, *94* (1), 013101–013103.

TENTATIVE COVER IMAGES

